Microsensors in Dynamic Backgrounds: Toward Real-Time Breath Monitoring

Kurt D. Benkstein, Baranidharan Raman, Christopher B. Montgomery, Carlos J. Martinez, and Steve Semancik

***Abstract*—We evaluated a microelectromechanical systems (MEMS) microsensor array with temperature-controlled chemi-resistive elements for use as a noninvasive clinical diagnostic tool to detect the presence or absence of trace amounts of disease biomarkers in simulated breath samples. The microsensor environment was periodically altered between air (78% N_2, 21% O_2 by volume, 20% relative humidity) and simulated breath (77% N_2, 16% O_2, 4% CO_2 by volume, 80% relative humidity) samples creating a dynamic background. Acetone, a disease marker for diabetes, was spiked into select simulated breath samples at relevant concentrations (0.5 μmol/mol to 8 μmol/mol) to pose a diagnostic problem for the sensor array. Using standard statistical dimensionality reduction and classification algorithms, we compared the ability of a variety of sensing materials to detect and recognize the disease marker. Our analyses indicate that the porous, doped nanoparticle materials (Sb:SnO_2 microshell films and Nb:TiO_2 nanoparticle films) are best for the recognition problem (acetone present versus absent), but that WO_3 and SnO_2 films are better at the quantification task (high versus low concentrations of acetone).**

***Index Terms*—Biological gases, gas detectors, microsensors, multidimensional signal processing, nanotechnology.**

I. Introduction

MICROSENSOR arrays, also known as "electronic noses," are generating increased interest as the need for small, low-cost chemical detectors rises. Potential applications include process control, homeland security, climate monitoring, and medical diagnostics. One of the least invasive medical screening methods may be exhaled breath analysis [1], [2]. Exhaled breath is largely composed of nitrogen, oxygen, carbon dioxide and water vapor (75%, 16%, 4%, and 4% by volume, respectively), but trace levels of volatile chemicals are also present that report on many physiological parameters including disease status. For example, the concentrations of ethane and pentane, generally present in nmol/mol levels in exhaled breath, can report on oxidative stress in the body (related to a variety of diseases), and acetone levels, at μmol/mol ranges, can provide information regarding diabetes [1], [3]. However, despite the diagnostic potential of breath, few clinical assays are available. Particularly significant would be the development of a low-cost, real-time, portable monitor that could be widely employed in examining rooms, or even in homes, to monitor disease/therapeutic progress noninvasively. The development of sensor arrays [4], [5], and chemiresistor (conductometric) microsensors specifically [6]–[8], for analysis of exhaled breath is an emerging field.

The breath analysis application poses significant challenges for microsensor measurements, however. Exhaled breath is extremely complex with hundreds of chemicals ranging in concentration from percent levels (nitrogen, oxygen, carbon dioxide, and water) to trace amounts less than 1 nmol/mol. Furthermore, healthy individuals will likely have some level of the marker analytes of interest in their exhaled breath, such that quantification is also important for accurate screening. The dynamic nature of exhaled breath is challenging in its own right: the ambient air has high oxygen partial pressure, whereas exhaled breath possesses lowered oxygen levels and increased carbon dioxide and humidity levels. Thus, the sensor array must be able to generate analytically robust datastreams (through careful choice of materials and operational modes) in order for the downstream signal processing modules to extract reliable chemical fingerprints for the identification and quantification of specific disease markers regardless of backgrounds and co-analytes.

In this paper, we propose a solution to this sensing problem using a microsensor array with chemiresitive elements. This type of technology and approach has shown promise for the detection of trace compounds in complex backgrounds [9], [10], largely driven by research performed for the homeland security sector. Here, we describe recent results demonstrating that the microsensor array can be used for the detection and quantification of acetone, a relevant disease biomarker for diabetes [1], [11], [12], in a simulated breath experiment. We evaluate several materials across a broad range of operating temperatures to demonstrate that there is sufficient analytical information in the microsensor datastreams to address the challenges of real-time breath monitoring.

II. Experimental

A. Microsensor Array

The microsensor array devices that we employed have been described in detail elsewhere [13]–[15]. Briefly, the arrays feature 16 individually addressable elements in a 4×4 configuration. Each element is a microhotplate platform, with elec-

Manuscript received December 03, 2008; revised February 13, 2009; accepted March 13, 2009. Current version published December 16, 2009. Official contribution of the National Institute of Standards and Technology; not subject to copyright in the United States. The work of B. Raman was supported by a joint National Institutes of Health (National Institute of Biomedical Imaging and Bioengineering)/National Institute of Standards and Technology joint postdoctoral fellowship from the National Research Council. The associate editor coordinating the review of this manuscript and approving it for publication was Prof. Cristina Davis.

K. D. Benkstein, B. Raman, C. B. Montgomery, and S. Semancik are with the National Institute of Standards and Technology, Gaithersburg, MD 20899-8362 USA (e-mail: kurt.benkstein@nist.gov).

C. J. Martinez is with the School of Materials Engineering, Purdue University, West Lafayette, IN 47907-2045 USA.

Color versions of one or more of the figures in this paper are available online at http://ieeexplore.ieee.org.

Digital Object Identifier 10.1109/JSEN.2009.2035738

SnO_2 375 °C 8 s	WO_3 1 drop	TiO_2 475 °C 30 s	Sb:SnO_2 μshell 2 drops
Nb:TiO_2 np 2 drops	Sb:SnO_2 μshell 2 drops	WO_3 1 drop	SnO_2 375 °C 8 s
TiO_2 475 °C 30 s	Nb:TiO_2 np 2 drops	SnO_2 375 °C 8 s	
WO_3 1 drop	TiO_2 475 °C 30 s	Sb:SnO_2 μshell 2 drops	Nb:TiO_2 np 2 drops

(a)

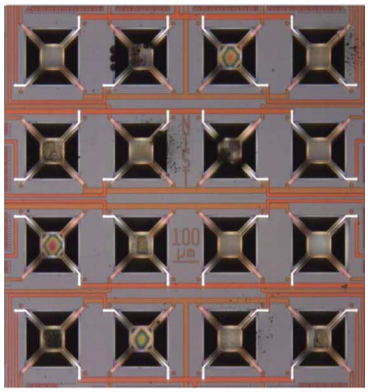

(b)

Fig. 1. (a) Schematic diagram showing the layout of the sensing films on the array, and their deposition conditions, and (b) an optical micrograph of the entire array.

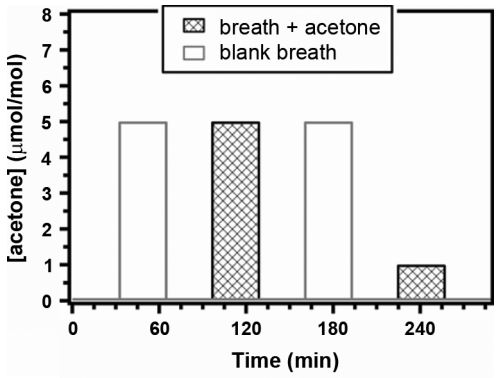

(a)

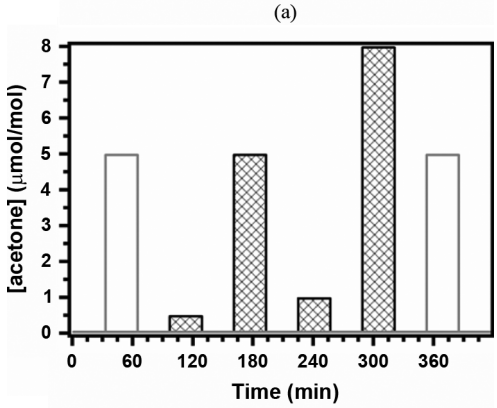

(b)

Fig. 2. The simulated-breath flow conditions and timing. The continuous background was 20% RH air and the breath samples contained 4% carbon dioxide, 16% oxygen and 80% RH. Shown in (a) is the simple experiment in which every second simulated breath was spiked with acetone. Shown in (b) is the second experiment with additional concentrations of acetone.

trical contacts at the surface. Sensing materials are prepared and/or deposited on each array element by chemical vapor deposition (tin(IV) oxide, SnO_2, and titanium(IV) oxide, TiO_2), or micropipetting (tungsten(VI) oxide, WO_3, antimony-doped (7% mass fraction) tin(IV) oxide, Sb:SnO_2, nanoparticle microshells, and niobium-doped (0.1 mol fraction) titanium(IV) oxide, Nb:TiO_2, nanoparticles) [16]–[18]. Sensing films studied via the array format included multiple copies of each material, with varied morphologies between the materials [9], [18]–[20]. Fig. 1(a) shows the layout of the materials and conditions for their growth/deposition (growth temperature and time for CVD films, number of drops for materials deposited by microcapillary pipetting). Drop volume for the microcapillary pipetting is estimated at < 650 pL.

B. Sensor Evaluation

The sensors were tested in a simulated-breath gas stream. The gas stream alternated between air (20% relative humidity) and simulated breath (77% N_2, 16% O_2, 4% CO_2 by volume, and 80% relative humidity with and without the target analyte: acetone, ranging in concentration from 0.5 μmol/mol to 8 μmol/mol). Zero-grade dry air was generated on-site, and acetone (500 μmol/mol, balance dry air), and carbon dioxide (22%, balance nitrogen) were mixed into the gas stream from cylinders. The humidified air was generated by passing dry air through a water bubbler at lab ambient temperature ($\mathrm{T} \approx 21$ °C); this gas stream was then mixed with the dilution-gas stream to either 20% or 80% of the total flow. The relative humidity of the humid-air stream ($> 95\%$ relative humidity) was confirmed with a hygrometer. The gas stream was controlled using a custom-built, automated flow system. The experimental flow profiles are shown in Fig. 2.

The responses of each microsensor element were probed at multiple temperatures to improve the analytical content. In this study, we cycled each microsensor element through 85 different temperatures from 60 °C to 480 °C in 5 °C increments.

To visualize the multivariate chemical sensor data (85 dimensions per sensor material) we used linear discriminant analysis (LDA) [21]. LDA is a supervised method that finds directions maximizing separation between different conditions and, at the same time, minimizing variance within each condition, i.e., eigenvectors of $S_W^{-1}S_B$ where S_W and S_B are within and between condition covariance matrices (only training samples are used to compute these matrices) [21].

To quantify the ability to differentiate different conditions, we performed a classification analysis using a k-nearest neighbor (KNN) classifier with twenty-fold validation. We also used a measure of cluster separability derived from LDA

$$J = \frac{\mathrm{trace}\,(S_B)}{\mathrm{trace}(S_B) + \mathrm{trace}(S_W)} \tag{1}$$

where S_W and S_B are the within-cluster and between-cluster scatter matrices, respectively, defined as follows:

$$S_W = \sum_{q=1}^{Q} \sum_{x \in \omega_q} (x - \mu_q)(x - \mu_q)^T \tag{2}$$

$$S_B = \sum_{q=1}^{Q} (\mu_q - \mu)(\mu_q - \mu)^T \tag{3}$$

$$\mu_q = \frac{1}{n_q} \sum_{x \in \omega_q} x \quad \text{and} \quad \mu = \frac{1}{n} \sum_{\forall x} x \tag{4}$$

where x is the linear projection of sensor response along $Q-1$ linear discriminant axes, Q is the number of conditions (four: background air, breath samples, breath samples with low concentrations of acetone, and breath samples with high concentrations of acetone), μ_q and n_q are the mean vector and number of examples for condition q, respectively, n is the total number of examples in the dataset, and μ is the mean vector of the entire distribution. Note that J increases monotonically as classes become increasingly more separable.

To determine which sensor features provide maximal discrimination between conditions (background, clean breath, low-concentration acetone and high-concentration acetone) and minimal variation within conditions as a function of sensor operating temperature, we used the modified t-statistic [21]:

$$t = \frac{|\mu_i - \mu_j|}{\sigma_i + \sigma_j} \tag{5}$$

where μ_i and σ_i are the mean and standard deviation of all of the measurements from a particular sensor at a particular temperature within condition "i," and μ_j and σ_j are the corresponding values within condition "j." The pair-wise t-statistic measure (six two class problems) was then averaged and plotted.

III. Results and Discussion

Fig. 1 shows the configuration of the sensor used for the results discussed here. The array features a variety of metal oxide films (five materials with three copies each), which operate as conductometric sensors [22]. One element of the 16-element array was left blank to provide a back-up sensor in the event that one of the active sensors failed, but was not used in these studies. The materials are all n-type metal oxides, but feature a variety of doping levels and morphologies ranging from relatively dense films deposited by chemical vapor deposition to highly porous structures produced by layer-by-layer assembly onto sacrificial microspheres [17]. These films were selected because they are generally responsive to analytes of interest for breath diagnostics, including volatile organic compounds [23] and simple inorganics like hydrogen cyanide and ammonia [9], [10].

Because metal oxide sensors like these are generally broadly selective, that is, they respond in varying degrees to many different analytes, they may be used to screen for multiple target biomarkers. However, in order to achieve discrimination between analytes, and general changes in background conditions,

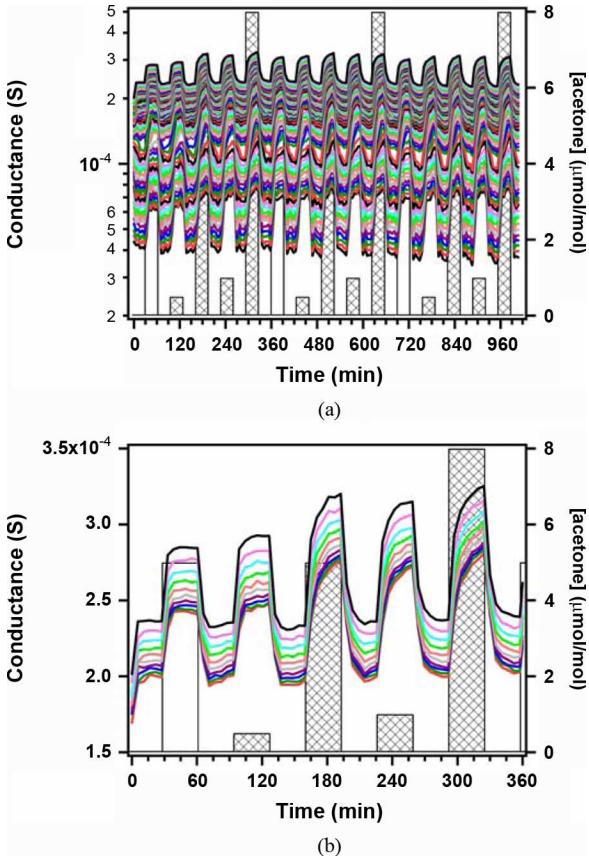

Fig. 3. Sensor data. Shown in (a) are the raw data collected from one microsensor (SnO_2 thin film) using the flow program in Fig. 2(b) Data collected at all 85 temperatures are shown (color-coded). Shown in (b) are data from select high temperatures ($T = 400\ ^\circ C$ to $480\ ^\circ C$, $\Delta T = 10\ ^\circ C$) for the microsensor during the first cycle of breath conditions. The concentration of acetone is shown for the crosshatched bars on the right axis.

it is necessary to induce analytical orthogonality in this microsensor array. For the complex problem of breath analysis, in addition to the varied materials, we have used the rapid temperature programming capabilities of these sensor platforms to sample many temperatures in a relatively short amount of time: 85 temperatures from 60 °C to 480 °C ($\Delta T = 5\ ^\circ C$) in $\approx$ 22 s for each microsensor element. While such a timescale is too long for real-time analysis of exhaled breath, we cannot know, *a priori*, which temperatures over that range for a particular sensing film and analyte will provide the most qualitative or quantitative analytical information. The type of large, dense temperature program employed allows us to explore the sensor responses as a function of operating temperature so that, at a later time, we may refine the temperature program to a select few, optimal temperatures that may be rapidly accessed (e.g., four or more temperatures in less than 1 s). Furthermore, since each microhotplate is individually addressable, we may use independently optimized temperatures for each of the five materials in the array.

For our experiments, we used a computer-controlled flow system to simulate an exhaled breath sampling experiment, represented in Fig. 2(a). The non-breath condition was air with 20% relative humidity, which represents background sampling conditions during inhalation. There were three simulated breath

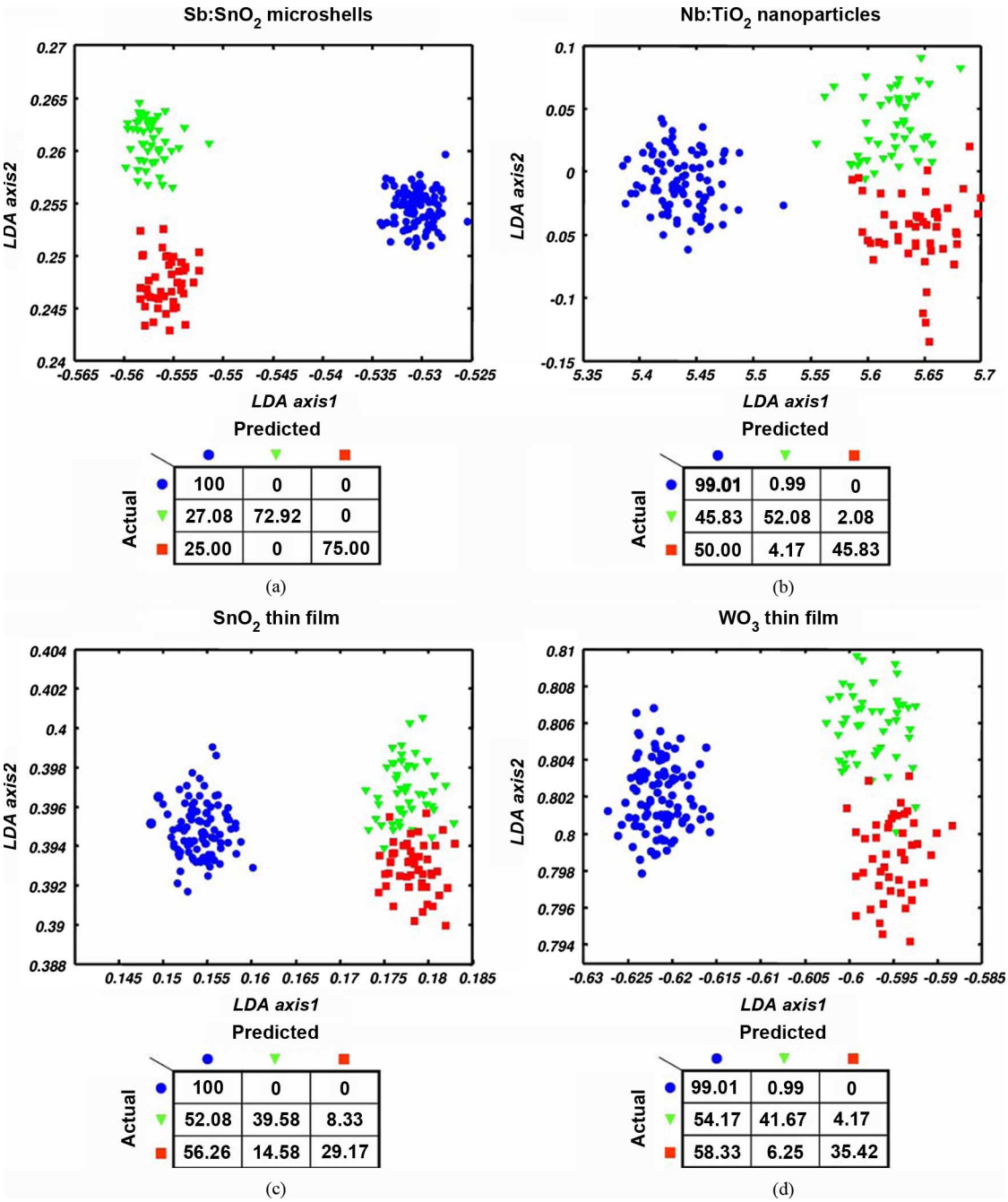

Fig. 4. (a–d) LDA plots of the data for the four best materials for the discrimination of exhaled breath from background air (•), and clean breath (▼) from acetone-spiked breath (■). Below the LDA plots are the corresponding classification confusion matrices for the four materials and the three conditions.

conditions: blank (4% carbon dioxide, 16% oxygen and the balance nitrogen with 80% relative humidity at room temperature), high acetone (5 μmol/mol of acetone with the blank mixture as the carrier), and low acetone (1 μmol/mol of acetone in the blank mixture). Follow-up experiments [Fig. 2(b)] used two additional concentrations of acetone in the simulated exhaled breath: 0.5 μmol/mol and 8 μmol/mol. The acetone levels cover the spread between the heightened levels for breath from subjects suffering diabetes and the lower levels for control subjects [12]. The flow rate for all conditions was maintained at 0.25 standard L/min. For our demonstration studies presented here, we have used an admittedly simplified simulated breath program. While the humidity level and temperature for the simulated breath samples are fixed or low, respectively, when compared to exhaled breath, we believe that the important demonstration at this stage for our microsensor array is its efficacy in a dynamic background: changing oxygen, humidity, and carbon dioxide levels. In order to be effective our sensor must be able to detect a trace amount of acetone while other conditions that also affect the sensor are simultaneously changing. Furthermore, previous studies have indicated that these types of microsensor arrays can adequately compensate for variations in relative humidity that would be encountered in real exhaled breath samples [10]. We also note that the inhalation/exhalation

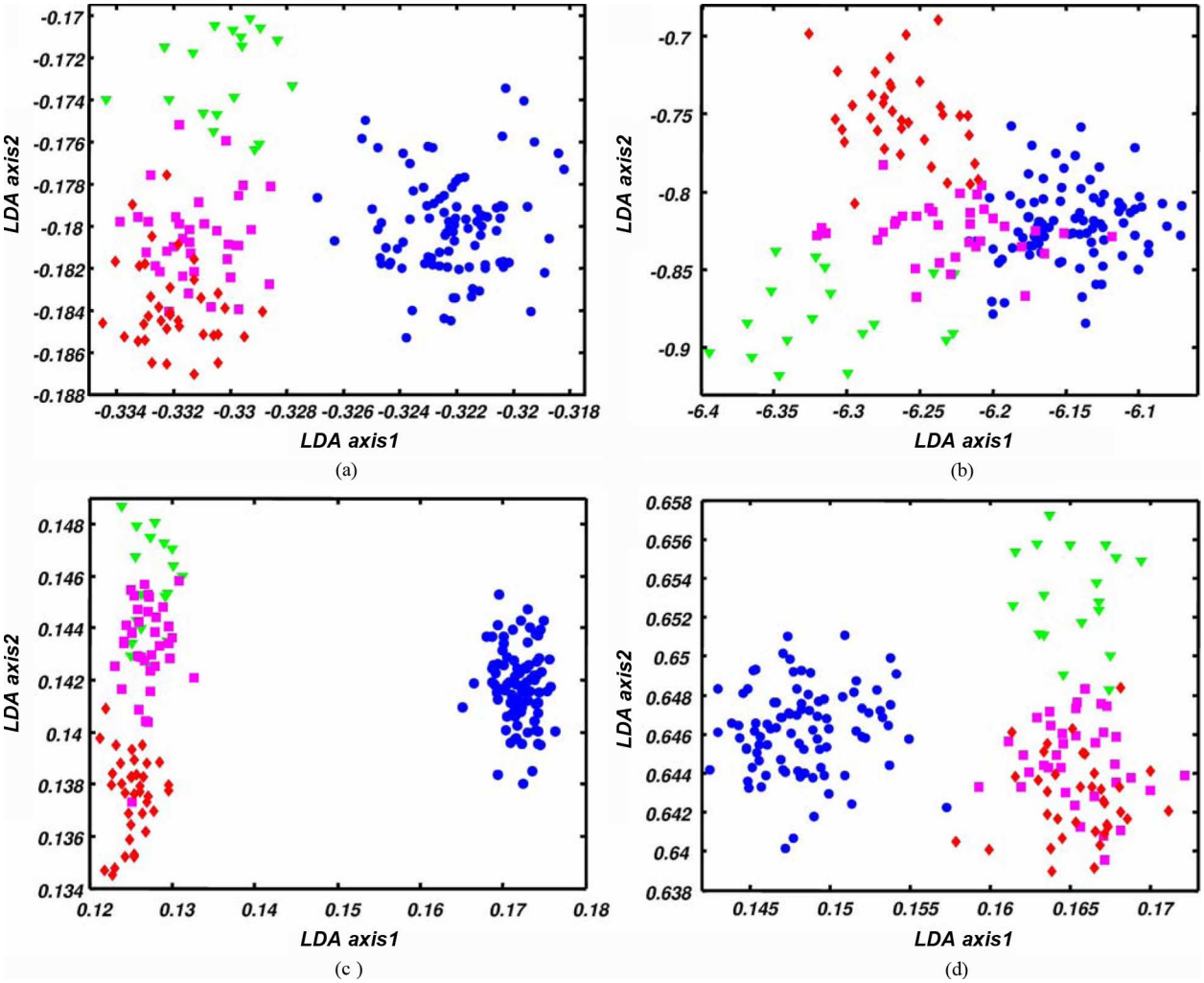

Fig. 5. LDA plots of the data for (a) a Sb:SnO_2 microshell film, (b) a Nb:TiO_2 nanoparticle film, (c) a SnO_2 thin film, and (d) a WO_3 film for the discrimination of exhaled breath from the background (•), and clean breath (▼) from low-concentration acetone-spiked breath (■) and high-concentration acetone-spiked breath (◆).

events are artificially long at 33 min. The long times provide sufficient data to do the initial classifications presented here, with the goal of optimizing the temperature programs for speed after these feasibility studies. Finally, we do not account for potential transients in the concentrations of analytes during the exhalation event.

Fig. 3 shows representative raw data collected from one of the microsensors using a SnO_2 thin film, running the simulated breath program depicted in Fig. 2(b). As seen in Fig. 3(a), the data stream is rich and complex, but differences between the various conditions are still evident. During the exhaled breath portion of the flow, the decrease in oxygen partial pressure and increase in humidity cause an increase of the conductance of the microsensor. Even the different levels of acetone appear to have some effect on the microsensor conductance, which is more clearly evident in the selected temperatures of Fig. 3(b). We also note that the response for this sensor appears to be slow, never reaching equilibrium during the simulated exhalations. However, this is not a problem, as long as the response transient is repeatable, which it appears to be, and the transient data may, in fact, yield more information than the equilibrium data [24]. To analyze and to gain the full utility of the large set of data collected across the entire array, we use standard multivariate signal processing techniques.

We first evaluated each of the chosen materials individually for their ability to distinguish response signatures for the three basic conditions: background samples, breath samples with no biomarkers, and breath samples with acetone. The plots in Fig. 4 show the LDA plots for microsensors using Sb-doped SnO_2 nanoparticle microshells and Nb-doped TiO_2 nanoparticles, and SnO_2 and WO_3 films, respectively. Each gas-phase condition is uniquely represented using a distinct symbol. The ability to differentiate the samples can be qualitatively determined by observing the separability of the samples belonging to the different conditions. Hence, from these results it is clear that the sensors based upon Sb:SnO_2 microshells and, to a lesser extent, the Nb:TiO_2 nanoparticles are best suited for determining whether acetone is present in the exhaled breath (please note the differences in scale for the four plots). The results for the titanium dioxide films are not shown or discussed because they did not show good separability between the conditions for this particular problem.

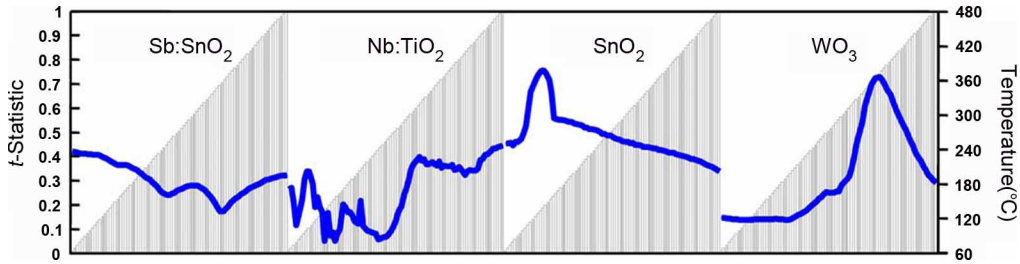

Fig. 6. Plots of the t-statistics (heavy blue lines, left axis) for the four best sensor materials (TiO_2 not shown) as a function of sensor operating temperature (gray steps, right axis) for the LDA plots in Fig. 5.

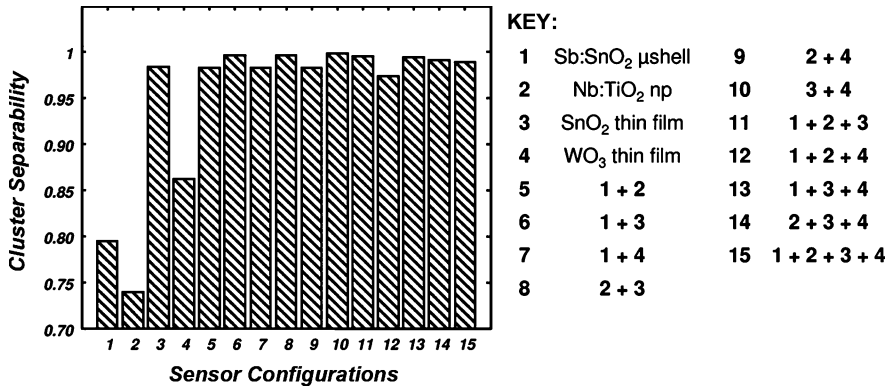

Fig. 7. Cluster separability (background, clean breath, low-concentration acetone, and high-concentration acetone) for individual sensor types and all combinations of sensor types.

We verified these qualitative results with a classification analysis using k-nearest neighbors ($k = 3$) with twenty-fold validation. In order to reduce false positives, we have enforced a decision rule that two predictions made using two consecutive measurements must agree in order to signal the presence of acetone. Fig. 4 shows the results of this classification analysis in confusion matrices below each of the LDA plots (diagonals represent correct classification and off-diagonals indicate false positives, above, and false negatives, below). The three different symbols are used to represent the conditions. The total classification accuracies for the films are: 87.31% (Sb-doped SnO_2), 79.79% (Nb-doped TiO_2), 68.08% (SnO_2), 69.54% (WO_3), and 58.38% (TiO_2, not shown). We note that copies of film types also had similar performance (not shown) and therefore we report only the best performance values here. Clearly, these results support the qualitative observations made using the LDA plots. These are also rather conservative estimates of the accuracy: first, we have required two consecutive measurements to agree, which effectively classifies transients (switches between background and breath) as background. Second, the LDA plots show total separability, while the confusion matrices are based upon training/validation analyses. Ultimately, these results demonstrate that sufficient analytical information may be obtained from most of the microsensors in the array to identify the presence of acetone in the sample stream, irrespective of the changing background conditions of a typical air stream to that of high humidity and low oxygen partial pressure in exhaled breath.

Having met the initial challenge of target recognition in a dynamic background, we next evaluated the ability of these microsensors to discriminate between different concentration levels of acetone in the simulated exhaled breath. For breath monitoring, such differentiation is necessary for diagnostic purposes, as only higher concentrations of a certain biomarker may indicate onset of a disease [3]. Fig. 5 shows the LDA plots from data collected using the flow program depicted in Fig. 2(b), where low (0.5 μmol/mol and 1 μmol/mol, square) and high (5 μmol/mol and 8 μmol/mol, diamond) concentrations of acetone are now also represented as distinct symbols. As can be clearly seen, the LDA plots are different from those in Fig. 4 for the different problem of separating acetone-spiked samples from the clean samples. For the semi-quantitative analyses here, the SnO_2 thin film sensor provides the best discrimination between different concentration levels of acetone, although there is still some overlap. Fig. 6 shows the t-statistics for this semi-quantitative problem. As seen, the two film-based sensors, SnO_2 and WO_3, both show high t-statistics, though in different temperature regimes (low and high temperatures, respectively). This demonstrates that the optimal temperature for a microsensor in the array is unique for the material and the problem being addressed. As expected from the LDA plots of Fig. 5, the nanoparticle-based sensors, as opposed to the thin film-based sensors, show only modest t-statistics for the concentration problem. Thus, the varied materials and operating temperatures in this microsensor array have distinct roles.

From the previous analyses, it may be hypothesized that a combination of the porous, doped nanoparticle materials with the SnO_2 thin films will provide an ideal array configuration to address the recognition and quantification requirements of this medical diagnostic problem. We demonstrate this by examining

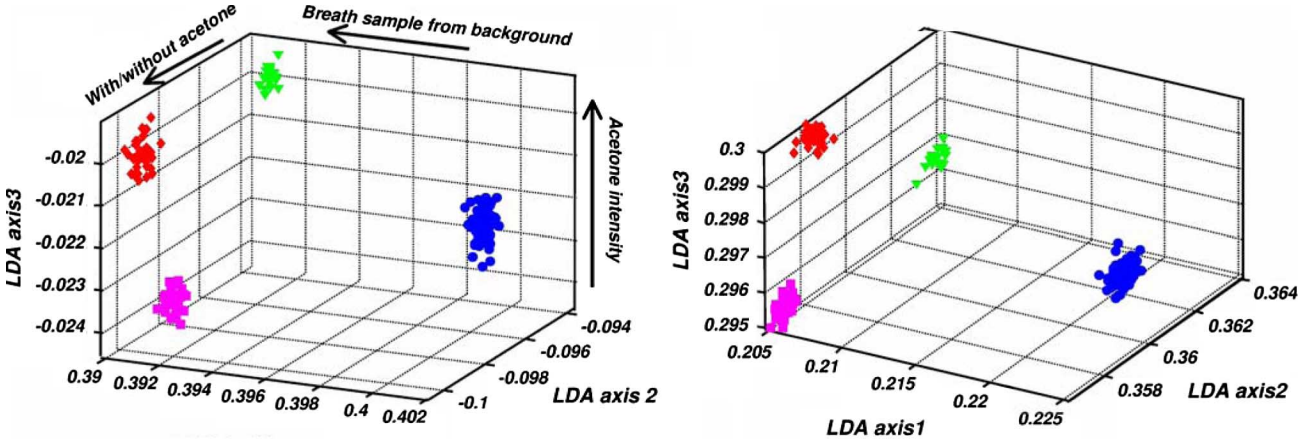

(a) (b)

Fig. 8. LDA plots of the data from (a) a SnO_2 thin film and a Sb:SnO_2 microshell film (**6** from Fig. 7), and (b) a SnO_2 thin film and a Nb:TiO_2 nanoparticle film (**8** from Fig. 7) for the discrimination of exhaled breath from the background (•), and clean breath (▼) from low-concentration acetone-spiked breath (■) and high-concentration acetone-spiked breath (⧫).

the cluster separability for the four best film types, and then look at the cluster separability when information from the individual sensors are used together (Fig. 7). For these analyses, we again included the expanded concentrations of acetone [Fig. 2(b)]. As seen from the cluster separability plots in Fig. 7, we do indeed observe that combinations of microsensors using pairs of elements with varied materials yields the highest separability. In particular, any pairing with the SnO_2 film appears to give superior separability. Interestingly, addition of more sensors to the mix does not improve the separability, and in many cases, actually makes it worse. Such a result could indicate averaging out of the discriminatory information when multiple films are combined. Fig. 8 provides a visual demonstration of these results using LDA plots for the two paired-microsensor analyses. As compared with Fig. 5, there is much better separability between each of the four conditions, with the pairing of the microsensor elements using a Sb-doped SnO_2 microshell film and a SnO_2 thin film yielding good discrimination between each condition [Fig. 8(a)]. Here, we have plotted the three LDA axes so that it is possible to observe the condition separability along the relevant axis.

IV. Conclusion

We have challenged a microsensor array with a simulated breath-monitoring experiment, focused on identifying and quantifying acetone, a disease biomarker for diabetes, in a dynamic background. Through the use of varied materials and the rapid survey of a broad temperature range, we have demonstrated that the microsensor array can cope with a changing background while still providing information on the quantity of acetone in the simulated exhaled breath. These results provide a demonstration of the power of a microsensor array for tackling the difficult challenge of real-time exhaled breath monitoring. However, certain hurdles must still be overcome, including the full complexity of exhaled breath and the rapid timing necessary if one is to achieve real-time monitoring. We believe that, based upon these initial promising results, microsensors may be successfully applied to the challenge of real-time monitoring of exhaled breath for disease biomarkers. We will continue to expand the library of disease biomarker measurements and will further refine and optimize the temperature program for each sensor material for analyte discrimination, quantification, and measurement speed.

Acknowledgment

The authors would like to thank D. C. Meier and Z. Boger for useful discussions, T. Risby for assistance in defining the breath-monitoring problem, and M. J. Carrier for technical assistance.

References

[1] T. H. Risby and S. F. Solga, "Current status of clinical breath analysis," *Appl. Phys. B*, vol. 85, pp. 421–426, 2006.
[2] A. D'Amico, C. Di Natale, R. Paolesse, A. Macagnano, E. Martinelli, G. Pennazza, A. Santonico, M. Bernabei, C. Roscioni, G. Galluccio, R. Bono, E. F. Agro, and S. Rullo, "Olfactory systems for medical applications," *Sens. Actuators B*, vol. 130, pp. 458–465, Mar. 2008.
[3] R. Mukhopadhyay, "Don't waste your breath," *Anal. Chem.*, vol. 76, pp. 273A–276A, 2004.
[4] A. Gelperin and A. T. C. Johnson, "Nanotube-based sensor arrays for clinical breath analysis," *J. Breath Res.*, vol. 2, 2008, 037015.
[5] B. P. J. de Lacy Costello, R. J. Ewen, and N. M. Ratcliffe, "A sensor system for monitoring the simple gases hydrogen, carbon monoxide, hydrogen sulfide, ammonia and ethanol in exhaled breath," *J. Breath Res.*, vol. 2, 2008, 037011.
[6] A. D. Aguilar, E. S. Forzani, L. A. Nagahara, I. Amlani, R. Tsui, and N. J. Tao, "Breath ammonia sensor based on conducting polymer nanojunctions," *IEEE Sens. J.*, vol. 8, no. 3, pp. 269–273, Mar. 2008.
[7] J. B. Yu, H. G. Byun, M. S. So, and J. S. Huh, "Analysis of diabetic patient's breath with conducting polymer sensor array," *Sens. Actuators B*, vol. 108, pp. 305–308, Jul. 2005.
[8] B. Fruhberger, N. Stirling, F. G. Grillo, S. Ma, D. Ruthven, R. J. Lad, and B. G. Frederick, "Detection and quantification of nitric oxide in human breath using a semiconducting oxide based chemiresistive microsensor," *Sens. Actuators B*, vol. 76, pp. 226–234, 2001.
[9] D. C. Meier, J. K. Evju, Z. Boger, B. Raman, K. D. Benkstein, C. J. Martinez, C. B. Montgomery, and S. Semancik, "The potential for and challenges of detecting chemical hazards with temperature-programmed microsensors," *Sens. Actuators B*, vol. 121, pp. 282–294, 2007.
[10] B. Raman, D. C. Meier, J. K. Evju, and S. Semancik, "Designing and optimizing microsensor arrays for recognizing chemical hazards in complex environments," *Sens. Actuators B: Chem.*, vol. 137, pp. 617–629, Apr. 2009.

[11] C. Wang and A. B. Surampudi, "An acetone breath analyzer using cavity ringdown spectroscopy: An initial test with human subjects under various situations," *Meas. Sci. Technol.*, vol. 19, p. 105604 (10 pgs.), Oct. 2008.
[12] C. H. Deng, J. Zhang, X. F. Yu, W. Zhang, and X. M. Zhang, "Determination of acetone in human breath by gas chromatography-mass spectrometry and solid-phase microextraction with on-fiber derivatization," *J. Chromatogr. B*, vol. 810, pp. 269–275, Oct. 2004.
[13] S. Semancik, R. E. Cavicchi, M. Gaitan, and J. S. Suehle, "Temperature-controlled micromachined arrays for chemical sensor fabrication and operation," U.S. patent 5,345,213, Sep. 6, 1994.
[14] S. Semancik and R. E. Cavicchi, "Kinetically controlled chemical sensing using micromachined structures," *Acc. Chem. Res.*, vol. 31, pp. 279–287, 1998.
[15] S. Semancik, R. E. Cavicchi, M. C. Wheeler, J. E. Tiffany, G. E. Poirier, R. M. Walton, J. S. Suehle, B. Panchapakesan, and D. L. DeVoe, "Microhotplate platforms for chemical sensor research," *Sens. Actuators B*, vol. 77, pp. 579–591, 2001.
[16] C. J. Taylor and S. Semancik, "Use of microhotplate arrays as microdeposition substrates for materials exploration," *Chem. Mater.*, vol. 14, pp. 1671–1677, 2002.
[17] K. D. Benkstein, C. J. Martinez, G. Li, D. C. Meier, C. B. Montgomery, and S. Semancik, "Integration of nanostructured materials with MEMS microhotplate platforms to enhance chemical sensor performance," *J. Nanopart. Res.*, vol. 8, pp. 809–822, 2006.
[18] C. J. Martinez, B. Hockey, C. B. Montgomery, and S. Semancik, "Porous tin oxide nanostructured microspheres for sensor applications," *Langmuir*, vol. 21, pp. 7937–7944, 2005.
[19] K. D. Benkstein and S. Semancik, "Mesoporous nanoparticle TiO_2 thin films for conductometric gas sensing on microhotplate platforms," *Sens. Actuators B*, vol. 113, pp. 445–453, 2006.
[20] K. D. Benkstein, B. Raman, D. L. Lahr, J. E. Bonevich, and S. Semancik, "Inducing analytical orthogonality in tungsten oxide-based microsensors using materials structure and dynamic temperature control," *Sens. Actuators B.*, vol. 137, pp. 48–55, Mar. 2009.
[21] R. Duda, P. E. Hart, and D. G. Stork, *Pattern Classification*. New York: Wiley-Interscience, 2000.
[22] N. Barsan and U. Weimar, "Conduction model of metal oxide gas sensors," *J. Electroceram.*, vol. 7, pp. 143–167, 2002.
[23] B. Raman, J. L. Hertz, K. D. Benkstein, and S. Semancik, "Bioinspired methodology for artificial olfaction," *Anal. Chem.*, vol. 80, pp. 8364–8371, 2008.
[24] R. Gutierrez-Osuna, A. Gutierrez-Galvez, and N. Powar, "Transient response analysis for temperature-modulated chemoresistors," *Sens. Actuators B*, vol. 93, pp. 57–66, 2003.

Kurt D. Benkstein received the B.S. degree (with distinction) in chemistry from Iowa State University, Ames, in 1995 and the M.S. and Ph.D. degrees in chemistry from Northwestern University, Evanston, IL, in 1996 and 2000, respectively.

He went to the National Renewable Energy Laboratory in 2000 as a Postdoctoral Researcher to study the relation between film morphology and electron transport in dye-sensitized nanoparticle solar cells. In 2003, he joined the National Institute of Standards and Technology, Gaithersburg, MD, as a Research Chemist to examine porous nanostructured materials in conductometric gas microsensors.

Baranidharan Raman received the B.S. degree (with distinction) in computer science from the University of Madras, Madras, India, in 2000 and the M.S. and Ph.D. degrees in computer science from Texas A&M University, College Station, in 2003 and 2005, respectively.

He is currently an NIH/NIST joint Postdoctoral Fellow in the Laboratory of Cellular and Synaptic Neurophysiology (NICHD), and the Process Sensing Group (NIST), National Institute of Standards and Technology, Gaithersburg, MD. His research interests include combining computational and electrophysiological approaches to study neural computations especially olfactory signal processing, sensor-based machine olfaction, machine learning, intelligent systems and robotics, human–computer interaction, and dynamical systems.

Christopher B. Montgomery began his career in 1983 with Petrarch Systems, Inc., as an organosynthetic chemist. He performed custom syntheses and provided technical service and analytical evaluations of novel silicones and silanes developed for the electronics, biomedical, and aerospace industries. In 1994, he joined SAIC developing protocols for self-assembled silane monomolecular layer formation (SAMMS), enabling hippocampal neuronal networks on patterned organosiloxy-modified surfaces. In 1997, he accepted a position with Commonwealth Scientific Corporation as a Process Engineer. Using ion beam technology, he developed and evaluated dielectric, diamond, optical and magnetic vacuum thin films serving the data storage, telecommunications, and biomedical communities. In 2000, he joined the National Institute of Standards and Technology (NIST), Gaithersburg, MD, preparing conductometric micro-gas sensor platforms. This includes micromachining of the micro-hotplate structure, as well as tailoring surface properties for adhesion, electrical conductivity, and catalysis via magnetron and ion beam sputtering. In addition, he performs vacuum thin films research for fabricating or modifying a variety of microelectromechanical devices.

Carlos J. Martinez was born in Rio Piedras, Puerto Rico. He received the B.S. degree in physics and electronics from the University of Puerto Rico, Humacao, in 1994 and the Ph.D. degree in materials science and engineering from the University of Illinois, Urbana–Champaign, in 2002, where he worked with Prof. Jennifer Lewis in the area of ceramic film formation.

In 2003, he received a National Research Council Postdoctoral fellowship to work with Dr. Steve Semancik in the Process Measurements Division at the National Institute of Standards and Technology, Gaithersburg, MD, developing porous nanoparticle structures for conductometric gas sensing. He then spend two years as a Visiting Scientist in Prof. D. Weitz's group at Harvard University, Cambridge, MA, where he worked in the area of double emulsion generation using microcapillary devices. He is now an Assistant Professor in the School of Materials Engineering at Purdue University, West Lafayette, IN.

Steve Semancik received the B.S. degree in physics from Rensselaer Polytechnic Institute, Troy, NY, and the M.Sc. and Ph.D. degrees in physics from Brown University, Providence, RI.

He is the Project Leader of the Chemical Microsensor Program at the National Institute of Standards and Technology (NIST), Gaithersburg, MD. His professional research career began as a National Research Council Postdoctoral Fellow and has been centered in the fields of surface science and sensor science. His recent work has focused on developing improved nanomaterials for chemical and biochemical sensing, and combining such high-performance materials with micromachined platforms to realize advanced microsensor devices and operating modes.

Dr. Semancik is an elected Fellow of both the American Physical Society and American Vacuum Society. He has served as a Member of the Editorial Board of two sensor journals, and is a Member of the Steering Committee of the International Meeting on Chemical Sensors.